Comprehensive analysis indicates DDX46 as a novel biomarker for the prognosis of lung adenocarcinoma

TINGTING BIAN[1,2*], MIAOSENG ZHENG[3*], TING WANG[4*], QING ZHANG[2], JIANGUO ZHANG[2], YIFEI LIU[2,5] and WENYU SHI[1,6]

[1]Suzhou Medical College of Soochow University, Suzhou, Jiangsu 215006, P.R. China; [2]Department of Pathology, Affiliated Hospital of Nantong University, Nantong, Jiangsu 226001, P.R. China; [3]Department of Pathology, The People's Hospital of Rugao, Rugao Hospital Affiliated to Nantong University, Nantong, Jiangsu 226001, P.R. China; [4]Department of Radiation Oncology, The Affiliated Cancer Hospital of Zhengzhou University and Henan Cancer Hospital, Zhengzhou, Henan 450008, P.R. China; [5]Medical School, Nantong University, Nantong, Jiangsu 226001, P.R. China; [6]Department of Oncology, Affiliated Hospital of Nantong University, Nantong, Jiangsu 226001, P.R. China

Received October 8, 2024; Accepted March 7, 2025

DOI: 10.3892/ol.2025.15038

Abstract. The expression levels of DEAD-box 46 (DDX46) are elevated in several malignancies; however, the function of DDX46 in lung adenocarcinoma (LUAD), including its expression patterns and functional implications, has not been fully elucidated. The present study primarily explores the potential role and underlying mechanism of DDX46 in the malignant progression of LUAD. The present study analyzed both publicly available databases and clinical specimens to assess DDX46 expression in LUAD and explore its prognostic significance. The findings demonstrated that elevated DDX46 expression was associated with a worse prognosis in patients with LUAD in comparison with a low DDX46 expression. Functional assays, including Cell Counting Kit-8, colony formation, 5-ethynyl-2'-deoxyuridine incorporation, flow cytometry, wound healing and Transwell assays, indicated that silencing DDX46 suppressed cancer cell migration, enhanced apoptosis, and induced G_0/G_1 phase cell cycle arrest. Moreover, DDX46 expression was correlated with the infiltration of T cells, natural killer cells and monocytes, as well as with several immune checkpoints and chemokines. Additionally, the results identified a marked association between DDX46 and the Wnt signaling pathway in LUAD. Low DDX46 expression was also demonstrated to be associated with increased drug responsiveness in patients. In conclusion, DDX46 holds promise as a dual-purpose marker for the diagnosis and therapy of patients with LUAD.

Correspondence to: Professor Yifei Liu, Department of Pathology, Affiliated Hospital of Nantong University, 20 Xisi Road, Nantong, Jiangsu 226001, P.R. China
E-mail: ntdxliuyifei@sina.com

Professor Wenyu Shi, Suzhou Medical College of Soochow University, 1 Shizi Street, Suzhou, Jiangsu 215006, P.R. China
E-mail: tdfyshiwenyu@163.com

*Contributed equally

Abbreviations: DDX46, DEAD-box 46; LC, lung cancer; LUAD, lung adenocarcinoma; TISCH, Tumor Immune Single Cell Hub; TIICs, tumor-infiltrating immune cells; RT-qPCR, reverse transcription-quantitative PCR; GSEA, Gene Set Enrichment Analysis; KEGG, Kyoto Encyclopedia of Genes and Genomes; APC, adenomatous polyposis coli; OS, overall survival

Key words: DDX46, LUAD, prognosis, immune, drug sensitivity

Introduction

Lung adenocarcinoma (LUAD) constitutes the predominant subtype of lung cancer (LC), comprising ~40% of all LC cases (1,2). The treatment of LUAD is tailored to the stage and severity of the disease, typically involving a combination of approaches such as surgery, radiotherapy, chemotherapy, immunotherapy and targeted therapy (3). Despite these diverse treatment strategies, the 5-year overall survival (OS) rate of patients with LUAD remains low, at ~15%, and few patients achieve complete remission (4,5). Accordingly, exploring the molecular basis of LUAD and seeking novel biomolecules for therapeutic purposes is a priority.

RNA helicases are essential regulators of several aspects of RNA metabolism, including transcription, RNA splicing, transport, storage, degradation, ribosome biogenesis and translation (6-8). By modulating the expression levels of oncogenes, RNA helicases contribute to tumorigenesis and advancement (9). Additionally, they are implicated in several pathological processes, such as neurological disorders, viral infections and aging (10). Among these, the DEAD-box (DDX) family stands out as a key group of human RNA helicases (11), with increasing evidence supporting their involvement in human tumorigenesis. Specifically, DDX46, located on chromosome 5q31.1, is a member of the DDX family. During pre-mRNA splicing and in the assembly of the spliceosome, DDX46 functions as a component of the 17S U2 small nuclear

ribonucleoprotein complex (12). Moreover, studies using zebrafish models have demonstrated that DDX46 is crucial for the multilineage differentiation of hematopoietic stem cells, as well as for the development of the digestive organs and the brain (9). Previous research has also reported that DDX46 is notably overexpressed in esophageal squamous cell carcinoma, where its silencing inhibits the Akt/IκBα/NF-κB signaling pathway, thereby inducing apoptosis (13). In osteosarcoma, DDX46 knockdown reduces tumor cell proliferation, migration and invasion (14). Furthermore, heightened expression of DDX46 has been reported in gastric cancer, where it is activated via the Akt/GSK/β-catenin pathway, promoting cancer cell proliferation and invasion (15). However, the relationship between DDX46 expression and LUAD progression remains unclear, and further investigation is needed to elucidate its potential role in LUAD.

The present study aimed to systematically assess the expression, pathological roles and the molecular basis of DDX46 in LUAD. To achieve this, a synergistic approach was employed that integrated bioinformatics analysis with experimental techniques.

Materials and methods

Public databases. The gene expression and clinical data from 535 LUAD samples (Table SI) and 59 normal lung tissue samples (16) were obtained from The Cancer Genome Atlas (TCGA) database (www.portal.gdc.cancer.gov/). Data processing was performed using R (version 3.6.3, The R Foundation for Statistical Computing; https://cran.r-project.org/src/base/R-3/R-3.6.3.tar.gz/) and Strawberry Perl (version 5.40.0.1; http://strawberryperl.com/).

Tissue specimens. A total of 20 pairs of fresh LUAD samples with their corresponding adjacent tissues, as well as 263 paraffin-embedded LUAD tissue blocks, were collected from the Affiliated Hospital of Nantong University (Nantong, China) between January 2012 and December 2015. The inclusion criteria were as follows: i) Patients pathologically diagnosed with LUAD; ii) no history of other malignant tumors; iii) sufficient samples available from the first visit for immunohistochemical analysis; iv) no prior anticancer treatment before surgery. Patients who did not meet the aforementioned criteria were not included in the present study. Tissue microarrays were carefully prepared by integrating the paraffin blocks with LUAD samples. The clinicopathological characteristics of the patients from which the samples were collected encompassed age, sex, smoking history, tumor differentiation, clinical stage, tumor stage (T), lymph node metastasis stage (N) and distant metastasis stage (M), along with survival duration and outcome. Prior to surgery, all patients provided written informed consent, confirming their clear understanding of the risks and benefits associated with the procedure. The study protocol and data collection were approved by the Ethics Committee of the Affiliated Hospital of Nantong University (approval no. 2022-L078).

Western blot analysis. Protein extraction was performed using RIPA buffer (cat. no. P0013B; Beyotime Institute of Biotechnology), followed by the measurement of total protein concentration in the samples. The total protein concentration in the samples was measured using a bicinchoninic acid protein assay kit (cat. no. P0010; Beyotime Institute of Biotechnology), following the manufacturer's instructions. This method ensures accurate quantification of protein content before proceeding with western blot analysis. For western blot analysis, equal amounts of total protein (20 μg/lane) were mixed with appropriate volumes of 5X SDS-PAGE loading buffer to ensure uniform loading volume across all lanes. Proteins were separated by SDS-PAGE on 10% gels and were then transferred onto a polyvinylidene difluoride (PVDF) membrane. The membrane was blocked with 5% non-fat milk in Tris-buffered saline with 0.1% Tween-20 at room temperature for 1 h to prevent non-specific binding. For antibody incubation, the PVDF membrane was then incubated overnight at 4˚C with the following primary antibodies: Anti-DDX46 (1:1,000; cat. no. ab72083; Abcam), anti-adenomatous polyposis coli (APC; 1:1,000, cat. no. ab40778; Abcam), anti-β-catenin (1:5,000; cat. no. 51067-2-AP, Proteintech Group, Inc.) and anti-β-actin (1:4,000; cat. no. 20536-1-AP; Proteintech Group, Inc.). Subsequently, the membrane was incubated with a HRP-conjugated goat anti-rabbit IgG secondary antibody (1:5,000; cat. no. SA00001-2; Proteintech Group, Inc.) at room temperature for 1 h. Protein signals were visualized using an enhanced chemiluminescence detection reagent (cat. no. 180-5001; Tanon Science and Technology Co., Ltd.). Densitometric analysis was performed using ImageJ software (version 1.53; National Institutes of Health).

Tissue chips immunohistochemical staining and analysis. The. LUAD and adjacent tissue sections were fixed in 10% neutral buffered formalin at room temperature for 24 h, embedded in paraffin and sectioned at a thickness of 4 μm. For immunohistochemical staining and analysis of tissue chips, antigen retrieval was performed using citrate buffer (pH 6.0) at 98˚C for 20 min, followed by washing with phosphate-buffered saline (PBS) and rehydration through a descending ethanol series (100, 95, 85 and 75%). Subsequently, the sections were incubated with 3% hydrogen peroxide for 20 min to inhibit endogenous peroxidase activity, followed by blocking with 5% normal rabbit serum (cat. no. ab7487; Abcam) at room temperature for 30 min. The sections were then incubated overnight at 4˚C with anti-DDX46 antibodies (1:200; cat. no. ab72083; Abcam), followed by incubation with an HRP-conjugated goat anti-rabbit IgG secondary antibody (1:500 dilution; cat. no. ab6721; Abcam) at room temperature for 1 h to enable signal detection. DDX46 staining was primarily localized in the nucleus of the cells. Immunohistochemical staining was evaluated and scored following the methodology described in our previous study (17).

Cell culture. The present study employed the following cell lines: BEAS-2B, PC-9, H1299, A549 and H1975, which were purchased from The Cell Bank of Type Culture Collection of The Chinese Academy of Sciences. BEAS-2B and A549 cells were maintained in Dulbecco's Modified Eagle Medium (cat. no. 11965092; Gibco; Thermo Fisher Scientific, Inc.), whereas PC-9, H1299, and H1975 cells were cultured in Roswell Park Memorial Institute (RPMI) 1640 medium (cat. no. 11875093; Gibco; Thermo Fisher Scientific, Inc.) The medium was

supplemented with 10% fetal bovine serum (FBS; cat. no. 10099141; Gibco; Thermo Fisher Scientific, Inc.) and 1% penicillin-streptomycin (cat. no. 15140122; Gibco; Thermo Fisher Scientific, Inc.) to prevent bacterial contamination. Cells were maintained at 37˚C in a humidified incubator with 5% CO_2.

Lentiviral transfection. Pre-packaged lentiviruses containing DDX46 short hairpin RNA (shRNA) and negative control (NC) shRNA were purchased from Shanghai GeneChem Co., Ltd. and were used directly for cell infection according to the manufacturer's instructions. The shRNAs were cloned into a GV248 plasmid backbone (U6-MCS-Ubiquitin-EGFP-IRES-puromycin). The following sequences were used: DDX46-*shRNA#*1, 5'-GATCCGCAGAAATCACCAGGCTCATACTCGAGTATGAGCCTGGTGATTTCTGCTTTTTG-3' and 5'-AATTCAAAAAGCAGAAATCACCAGGCTCATACTCGAGTATGAGCCTGGTGATTTCTGCG-3'; DDX46-shRNA#2, 5'-GATCCCCTGTGCTGGTCTATGATGTACTCGAGTACATCATAGACCAGCACAGGTTTTTG-3' and 5'-AATTCAAAAACCTGTGCTGGTCTATGATGTACTCGAGTACATCATAGACCAGCACAGGG-3'; and NC-shRNA, 5'-TTCTCCGAACGTGTCACGT-3' and 5'-AAGAGGCTTGCACAGTGCA-3'. According to the manufacturer's instructions, PC-9 and H1299 cells were infected with concentrated lentiviruses containing either NC-shRNA or DDX46-shRNA at a multiplicity of infection of 40 in serum-free RPMI-1640 medium supplemented with 8 μg/ml polybrene. After 24 h, the supernatant was replaced with RPMI-1640 medium containing 10% FBS. After 72 h of infection, the cells were selected with puromycin at a concentration of 2 μg/ml for 3 days, and were maintained in medium containing 1 μg/ml puromycin for subsequent experiments. The efficiency of NC-shRNA or DDX46-shRNA in infected cells was assessed by reverse transcription-quantitative polymerase chain reaction (RT-qPCR).

Cell counting kit-8 (CCK8) assay. After transfecting NC-shRNA and DDX46-shRNA into LUAD cells (PC-9 and H1299) for 48 h, the cells were collected, resuspended and seeded at a concentration of $1x10^3$ cells/well in a 96-well plate. The plate was subsequently incubated at 37˚C with 5% CO_2 for 24-96 h. Following the incubation period, 10 μl CCK-8 reagent (cat. no. C0042; Beyotime Institute of Biotechnology) was added to each well, and the plate was incubated for an additional 2.5 h to allow the reagent to react with the viable cells. Microplate readers were used to measure the absorbance (optical density) of each well at 450 nm, and cell viability was calculated from the absorbance value.

5-ethynyl-2'-deoxyuridine (EdU) assay. After transfecting NC-shRNA and DDX46-shRNA for 48 h, H1299 and PC-9 cells ($4x10^4$ cells/well) were seeded in a 24-well plate and incubated with EdU solution (cat. no. C0075S; Beyotime Institute of Biotechnology) for 2 h. Following fixation with 4% paraformaldehyde for 15 min at room temperature, cells were permeabilized for 15 min with 0.3% Triton X-100. The cells were then incubated in the dark for 30 min at room temperature. Subsequently, the cells were stained with Hoechst for 10 min at room temperature (Beyotime Biotechnology of Biotechnology) and examined under a fluorescence microscope to record the results.

Colony formation assay. Cells transfected with sh-NC and sh-DDX46 were separately seeded at a density of 1,000 cells/well in a 6-well plate and incubated at 37˚C with 5% CO_2 for 2 weeks. Once colonies had formed, at room temperature the cells were fixed with formaldehyde for 20 min and then stained with 0.5% crystal violet solution for 10 min. Colonies were defined as cell clusters containing ≥50 cells, indicating proliferation from a single cell. Stained colonies were quantified using ImageJ (version 1.53) with the Colony Counter plugin.

Detection of cell cycle. LUAD cells transfected with sh-NC and sh-DDX46 were trypsinized, fixed with 70% ethanol at -20˚C, cultured for 24 h, washed with pre-chilled PBS at 4˚C, and then incubated with 500 μl PI/RNAse solution (cat. no. 550825; BD Biosciences) for 30 min at 37˚C in the dark. Cell cycle analysis was performed using a BD FACSCanto II (BD Biosciences), and the data were analyzed using FlowJo v10.8 (BD Biosciences).

Wound healing assay. A wound was created by scratching the sh-NC- and sh-DDX46-transfected cells in 6x-well plates using a 100-μl pipette tip. After scratching, the cells were washed with PBS to remove debris and then cultured in serum-free medium to minimize proliferation during the assay. A microscope was used to observe the healing progress at 0, 24 and 48 h and the wound healing area percentage was determined using Image J software (version 1.53). At the start of the study, cells on either side of the wound were at 100% confluence. Microscopic images were captured using an Olympus IX73 inverted fluorescence microscope (Olympus Corporation).

Transwell assay. Cell migration was evaluated using Transwell chambers (Corning, Inc.) with an 8-μm pore size. Initially, sh-NC- and sh-DDX46-transfected cells were suspended in incomplete medium and then seeded at a density of $2x10^4$ cells/well in the upper Transwell chamber. The lower chamber was filled with RPMI-1640 and 10% FBS, and the cell culture was incubated at 37˚C with 5% CO_2 for 24 h. After the cells migrated through the chamber membrane, they were fixed with 4% paraformaldehyde at room temperature for 15 min and stained with 0.1% crystal violet solution for 10 min. Subsequently, cell images were captured using an Olympus IX73 inverted fluorescence microscope, and the number of cells in the lower chamber was counted.

RT-qPCR. LUAD cells transfected with sh-NC and sh-DDX46 were lysed with TRIzol™ reagent (cat. no. 15596026CN; Thermo Fisher Scientific, Inc.), following the manufacturer's instructions. Chloroform, isopropanol and 75% ethanol were then added to the cells, and the total RNA was extracted. A PCR machine (Applied Biosystems 2720 Thermal Cycler; Thermo Fisher Scientific, Inc.) was used to run at the following conditions to obtain cDNA using RT (cat. no. R222-01; Vazyme Biotech Co., Ltd.): 42˚C for 1 h and 70˚C for 10 min. SYBR Green (SYBR™ Green Master Mix; Thermo Fisher Scientific, Inc.) was used for qPCR detection and the qPCR thermocycling

conditions included an initial denaturation step at 95˚C for 2-3 min, followed by 40 cycles at 95˚C for 10-15 sec and 60˚C for 30 sec with fluorescence detection. Melt curve analysis was performed at 95˚C for 15 sec, 60˚C for 1 min and a gradual increase to 95˚C (0.1˚C/sec) with continuous fluorescence acquisition. The forward and reverse sequences used were as follows: DDX46 forward, 5'-AAGCTCTTGAATTGTCAGGGA-3' and reverse, 5'-CCCTTACCAGAGAACCCACT-3'; and β-actin forward, 5'-AGTTGCGTTACACCCTTTCTTG-3' and reverse, 5'-GCTGTCACCTTCACCGTTCC-3'. The $2^{-\Delta\Delta Cq}$ method was used for relative quantification of gene expression, with normalization to β-actin as the internal reference gene (18).

TUNEL assay. The apoptotic rate of LUAD cells transfected with sh-NC and sh-DDX46 was assessed using TUNEL staining. The control and DDX46 knockdown groups were fixed with 4% paraformaldehyde for 30 min at room temperature, followed by permeabilization with 0.3% Triton X-100 for 5 min. Subsequently, the cells were incubated with TUNEL detection solution at 37˚C for 60 min in the dark. Subsequent Hoechst staining for 15 min at room temperature facilitated cell imaging using a fluorescence microscope. The mounting medium used for fluorescence microscopy was Fluoromount-G™ (Thermo Fisher Scientific, Inc.) and 10 random fields per sample were observed to ensure statistical reliability.

Single-cell analysis of DDX46. The Tumor Immune Single-cell Hub (TISCH; www.tisch.comp-generations.org/home/) is a comprehensive database designed to facilitate several single-cell analyses, containing nearly 190 samples (19). The present study specifically focused on the distribution of DDX46 across different cell subpopulations in LUAD; therefore, single-cell RNA sequencing data was downloaded from the GSE117570 dataset (20) within the TISCH database to assess DDX46 expression levels across different cell types. The expression levels of DDX46 were quantified and visualized using scatter and violin plots.

Immune infiltration analysis. Utilizing CIBERSORT (version 1.0; https://cibersort.stanford.edu/), an analysis was performed to assess the correlation between DDX46 and tumor-infiltrating immune cells (TIICs), evaluating the connection between DDX46 expression levels and the prevalence of eight distinct types of TIICs (21). To analyze the correlation between DDX46 expression and immune checkpoints and chemokines, gene expression levels were extracted for seven immune checkpoints and 40 chemokines. Spearman correlation analysis was performed and correlation heatmaps were generated using the reshape2 (version 1.4.4; https://cran.r-project.org/package=reshape2), corrplot (version 0.95; https://cran.r-project.org/package=corrplot), boot (version 1.3-28.1; https://cran.r-project.org/package=boot), and ggplot2 packages (version 3.5.1; https://cran.r-project.org/package=ggplot2) in R (version 4.1.3; https://www.r-project.org/).

Enrichment analysis. Enrichment analysis and the functional annotation of genes was performed using the Gene Set Enrichment Analysis (GSEA) website (www.software.broadinstitute:gsea/index.jsp). GSEA is a widely utilized method for gene enrichment analysis that assesses the enrichment levels of predefined gene sets within specific biological processes, signaling pathways or diseases by evaluating their correlation with these processes (22). GSEA enrichment analysis was performed to annotate the sample genetics with Kyoto Encyclopedia of Genes and Genomes (KEGG; https://www.kegg.jp/). The screening criteria were as follows: $P<0.05$ and false discovery rate (FDR) <0.05.

Drug sensitivity analysis of DDX46. The largest public pharmacogenomics resource, the Cancer Drug Sensitivity Genomics website (www.cancerrxgene.org/), provided the anticancer drug dataset used in the present study (23). To assess the association between IC_{50} values of diverse anticancer drugs and DDX46 expression groups, the oncoPredict package 1.2 (https://cran.r-project.org/web/packages/oncoPredict/index.html) was used. Subsequently, statistical analysis of drug sensitivity within these groups was performed using the R package 'pRRophetic' 0.5 (https://github.com/paulgeeleher/pRRophetic) to assess differences in drug response levels among patients in different risk groups.

Statistical analysis. Data are presented as the mean ± standard deviation or mean ± standard error of the mean for continuous variables, whereas categorical variables are presented as percentages or frequencies. Three independent biological replicates (n=3) were performed for *in vitro* experiments. Paired t-tests were used to compare normal and malignant tissues from the same patient, whilst unpaired t-tests were employed for comparisons between two independent groups. One-way analysis of variance (ANOVA) was performed to compare ≥3 groups. Dunnett's multiple comparison test was subsequently applied to compare each experimental group with the control, whilst controlling for the familywise error rate, provided the ANOVA result revealed significant differences ($P<0.05$). The Kaplan-Meier method and log-rank test were used to evaluate the relationship between lung cancer prognosis and DDX46 expression levels, comparing both low and high expression groups. $P<0.05$ was considered to indicate a statistically significant difference. All statistical analyses were performed using SPSS 26 (IBM Corp.) and GraphPad Prism 10 (Dotmatics).

Results

Increased expression of DDX46 in LUAD samples. At the proteome level, DDX46 was demonstrated to be significantly overexpressed in several tumor tissues, including lung cancer, compared with that in normal tissues (Fig. 1A). Specifically in LUAD, DDX46 expression was revealed to be significantly higher in LUAD tissues compared with that in normal lung tissues (Fig. 1B and C). Furthermore, western blot analysis of eight LUAD samples and matched normal lung tissues further demonstrated a marked increase in DDX46 protein levels in LUAD tissues (Fig. 1D).

Association between DDX46 expression and clinicopathological characteristics, along with the prognosis of patients with LUAD. To assess the relationship between DDX46 expression and clinicopathological characteristics, as well as patient prognosis in LUAD, immunohistochemical staining was performed on 263 LUAD samples. The results revealed that DDX46 was predominantly localized in the nucleus and had notably higher

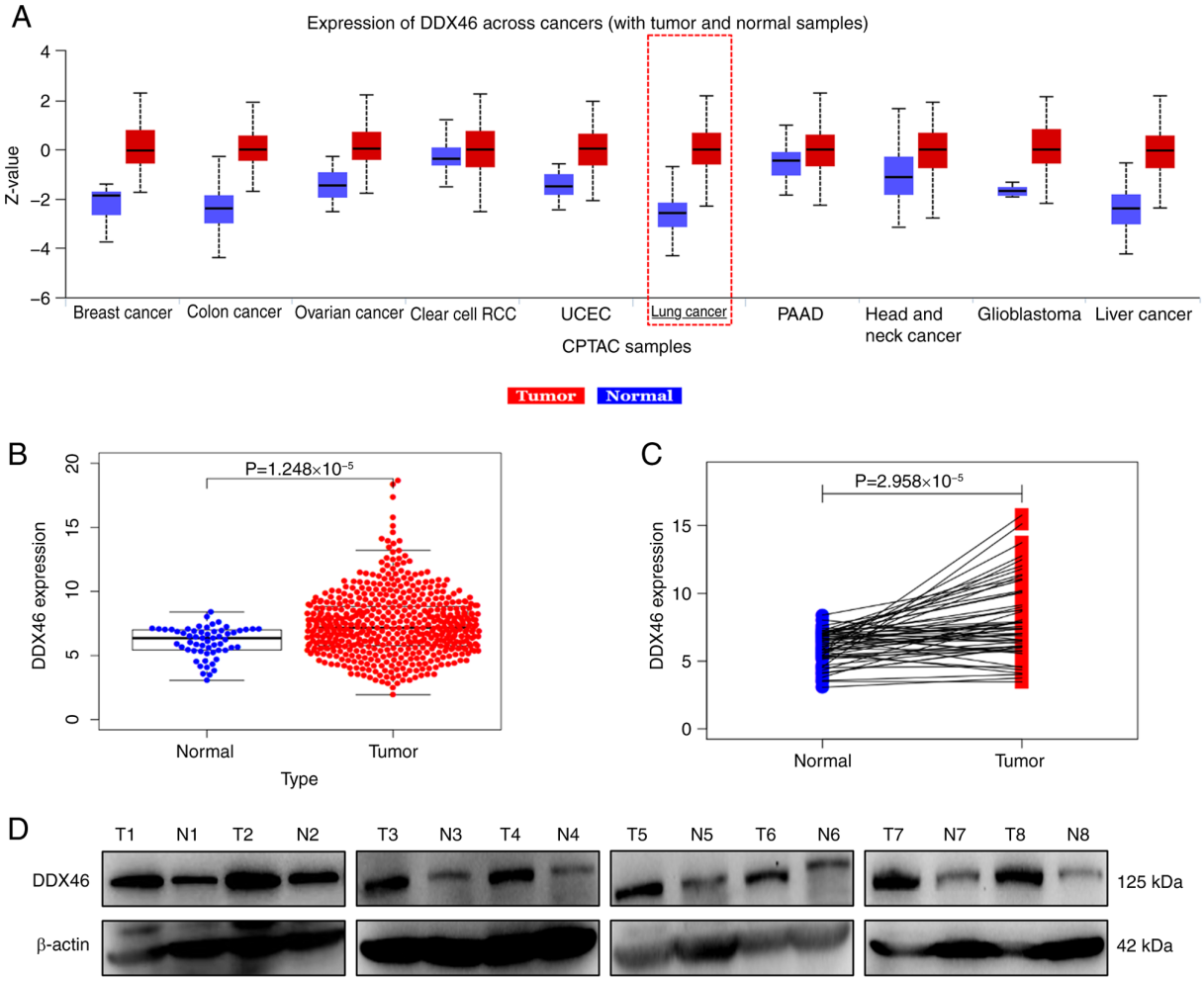

Figure 1. Expression of DDX46 in LUAD and adjacent normal tissues. (A) Expression of DDX46 in cancerous and adjacent normal tissues across several tumors. (B) TCGA analysis of DDX46 gene expression in LUAD and normal lung tissues. (C) TCGA paired analysis of DDX46 expression in LUAD adjacent and cancer tissues. (D) Western blot of DDX46 protein expression in LUAD adjacent and cancer tissues. DDX46, DEAD-box 46; LUAD, lung adenocarcinoma; RCC, renal cell carcinoma; UCEC, uterine corpus endometrial carcinoma; PAAD, pancreatic adenocarcinoma; CPTAC, Clinical Proteome Tumor Analysis Consortium; TCGA, The Cancer Genome Atlas.

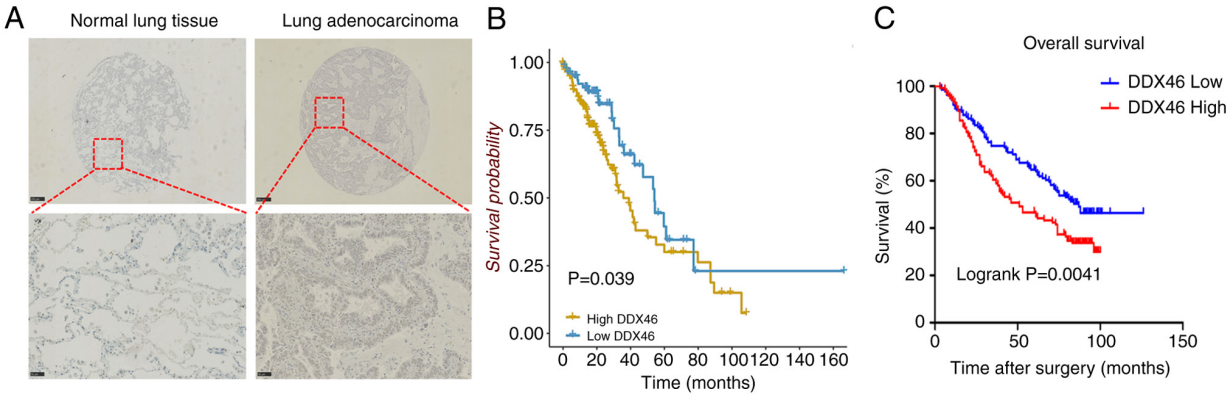

Figure 2. Immunohistochemical staining and KM survival analysis of LUAD tissues. (A) Immunohistochemical staining of LUAD and normal lung tissues (scale bars: Upper panels, 250 μm; lower panels, 50 μm). KM curves of the DDX46 high and low expression groups of (B) patients with LUAD in The Cancer Genome Atlas database and (C) the LUAD tissue microarray. KM, Kaplan-Meier; LUAD, lung adenocarcinoma; DDX46, DEAD-box 46.

expression levels in LUAD tissues than in adjacent non-tumor tissues (Fig. 2A). Moreover, DDX46 expression was significantly associated with stage (P=0.007) and T classification (P=0.036), whilst no statistically significant associations were demonstrated for age, sex, smoking history, differentiation degree or N classification (all P>0.05) (Table I).

Kaplan-Meier analysis of data from the TCGA database indicated that patients exhibiting high DDX46 expression

Table I. Association between DEAD-box 46 expression and pathological parameters of lung adenocarcinoma.

		DDX46 expression, n		
Clinical parameter	Total, n	Low	High	P-value
Age				0.403
≤60 years	108	60	48	
>60 years	155	78	77	
Sex				0.210
Male	160	79	81	
Female	103	59	44	
Smoking				0.548
Nonsmoker	212	113	99	
Smoker	51	25	26	
Stage				0.007[a]
I + II	189	109	80	
III + IV	74	29	45	
Differentiated degree				0.871
I + II	186	97	89	
III	77	41	36	
T classification				0.036[b]
1 + 2	236	129	107	
3 + 4	27	9	18	
N classification				
N0	149	84	65	0.147
N1 + N2	114	54	60	

[a]P<0.01; [b]P<0.05. DDX46, DEAD-box 46; T, tumor stage; N, lymph node stage.

experienced significantly worse OS than those with low DDX46 expression (P=0.039; Fig. 2B). Further analysis on tissue chips corroborated this finding, revealing a significant negative association between DDX46 expression and OS in patients with LUAD (P=0.0041; Fig. 2C). Moreover, DDX46 expression was demonstrated to be a significant independent prognostic factor in LUAD (Table II). High DDX46 expression was significantly associated with a worse prognosis, with a hazard ratio (HR) of 1.068 in univariate analysis (P=0.004) and 1.056 in multivariate analysis (P=0.022), underscoring its prognostic impact even when controlling for other variables. Although tumor stage was also revealed to be a significant independent prognostic factor (univariate HR=1.321; P=0.001 and multivariate HR=1.567; P=0.009), the consistent association of DDX46 with survival points to its unique role as a potential standalone prognostic biomarker for LUAD.

H1299 and PC-9 cells transfected with lentivirus to knockdown DDX46 expression. Initially, the expression of DDX46 was assessed in human normal lung epithelial BEAS-2B cells and LUAD cell lines, including PC-9, H1299, H1975 and A549. DDX46 expression was demonstrated to be significantly higher in PC-9, H1299, A549 and H1975 cells compared with that in BEAS-2B cells (Fig. 3A). Based on these findings, H1299 and PC-9 cells were selected for transfection with lentiviral vectors, including shNC, shDDX46#1 and shDDX46#2, and observation of the fluorescence signal intensity confirmed successful viral transfection (Fig. 3B). Subsequent RT-qPCR and western blot analyses revealed a significant reduction in DDX46 mRNA and protein levels in H1299 cells, in comparison with the negative controls (Fig. 3C and D). Similarly, DDX46 RNA and protein levels were significantly decreased in PC-9 cells, in comparison with the negative controls (Fig. 3E and F).

DDX46 knockdown inhibits the proliferation potential of LUAD cells. CCK-8 assays, colony formation analyses and EdU experiments indicated a significantly lower proliferation activity in the shDDX46 group compared with that in the NC group (Fig. 4A-C). Subsequently, flow cytometric analysis of the cell cycle showed that knocking down the DDX46 gene led to an increase in the proportion of G_0/G_1 phase cells and a decrease in G_2/M phase cells, indicating a cell cycle arrest in the G_0/G_1 phase (Fig. 4D).

Knockdown of DDX46 expression suppresses the migration of LUAD cells. To assess the role of DDX46 in the migration of LUAD cells, Transwell and wound healing assays were performed using H1299 and PC-9 cells. The Transwell assay demonstrated a significant reduction in the number of both DDX46-knockdown H1299 and PC-9 cells migrating through the polycarbonate membrane, compared with in the control group (Fig. 5A). Similarly, the wound healing assay revealed

Table II. Univariable and multivariable Cox regression analyses.

	Univariate analysis		Multivariate analysis	
Clinicopathologic parameter	HR (95% CI)	P-value	HR (95% CI)	P-value
Age	1.017 (1.000-1.035)	0.055	1.017 (0.999-1.035)	0.062
Stage	1.321 (1.112-1.563)	0.001[a]	1.567 (1.121-2.191)	0.009[b]
T classification	1.240 (1.043-1.475)	0.015[c]	1.012 (0.813-1.259)	0.916
N classification	1.166 (0.960-1.416)	0.122	0.782 (0.564-1.085)	0.142
M classification	1.139 (0.503-2.580)	0.754	0.528 (0.208-1.338)	0.178
DDX46 expression	1.068 (1.02-1.117)	0.004[b]	1.056 (1.008-1.108)	0.022[c]

[a]P<0.001; [b]P<0.01; [c]P<0.05. T, tumor stage; N, lymph node stage; M, metastasis stage; DDX46, DEAD-box 46; HR, hazard ratio; CI, confidence interval.

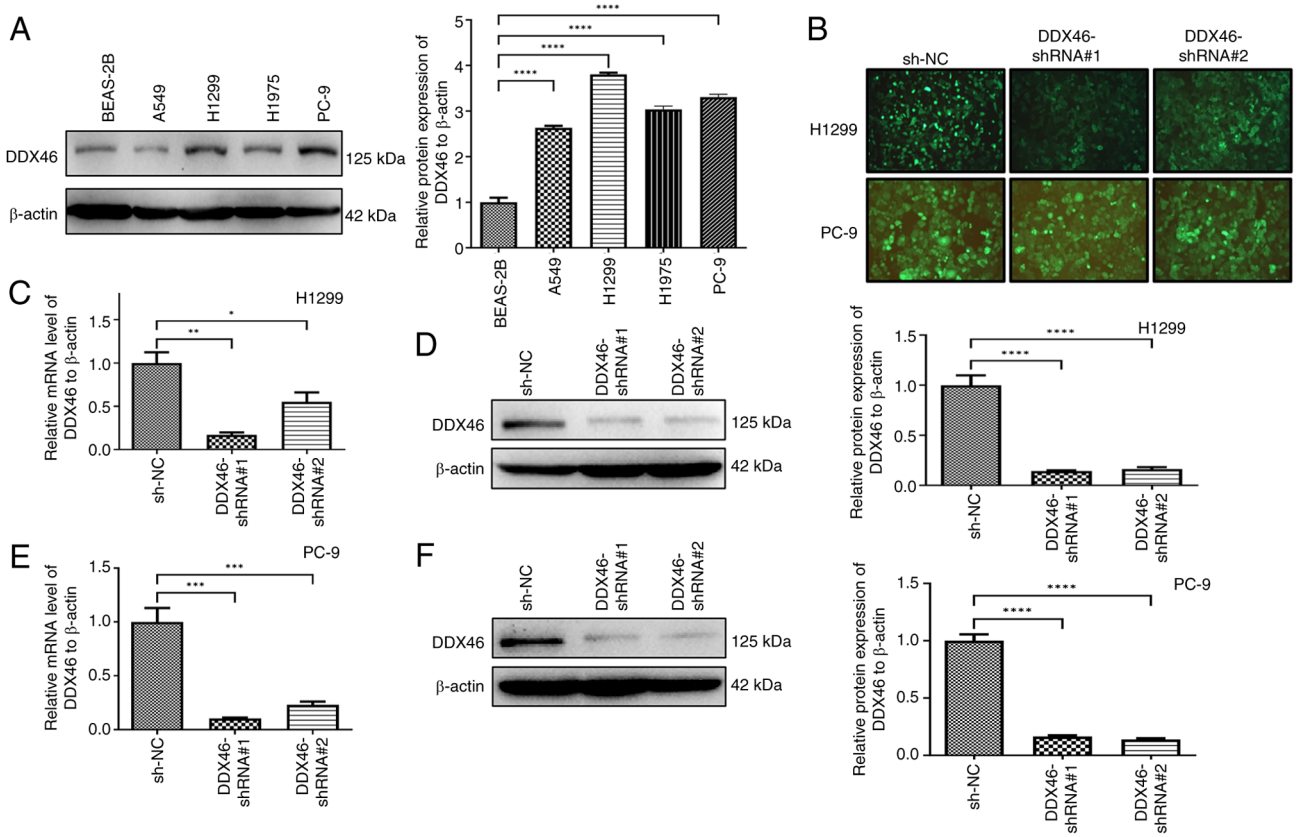

Figure 3. Expression of DDX46 in several cell lines and the effect of silencing DDX46 *in vitro*. (A) DDX46 protein levels in BEAS-2B, A549, H1975, H1299 and PC-9 cell lines. (B) The knockdown DDX46 lentiviral vector was transfected into H1299 and PC-9 cells, with the intensity of the green fluorescence signal serves as an indicator of the efficiency of the corresponding lentivirus transfection (magnification, x200). The effect of silencing DDX46 in H1299 cells was assessed using (C) RT-qPCR and (D) western blotting, and the effect of silencing DDX46 in PC-9 cells was evaluated using (E) RT-qPCR and (F) western blotting. *P<0.05; **P<0.01; ***P<0.001; ****P<0.0001. DDX46, DEAD-box 4; RT-qPCR, reverse transcription-quantitative PCR; ns, no significance; NC, negative control; shRNA, short hairpin RNA.

significantly reduced wound closure in H1299 and PC-9 cells with DDX46 knockdown compared with in the control group (Fig. 5B). Altogether, these findings imply that knockdown of DDX46 expression attenuates the migration of H1299 and PC-9 cells.

Knockdown of DDX46 expression promotes apoptosis in LUAD cells. TUNEL staining was used to evaluate the impact of DDX46 knockdown on the apoptosis of LUAD cells. The results revealed that, relative to the control group, DDX46 knockdown was associated with a significant increase in the rate of apoptosis in both H1299 and PC-9 cells (Fig. 5C).

DDX46 regulates the Wnt signaling pathway in LUAD cells. To further elucidate the potential mechanism of the DDX46 gene in LUAD samples, TCGA-LUAD data was subjected to

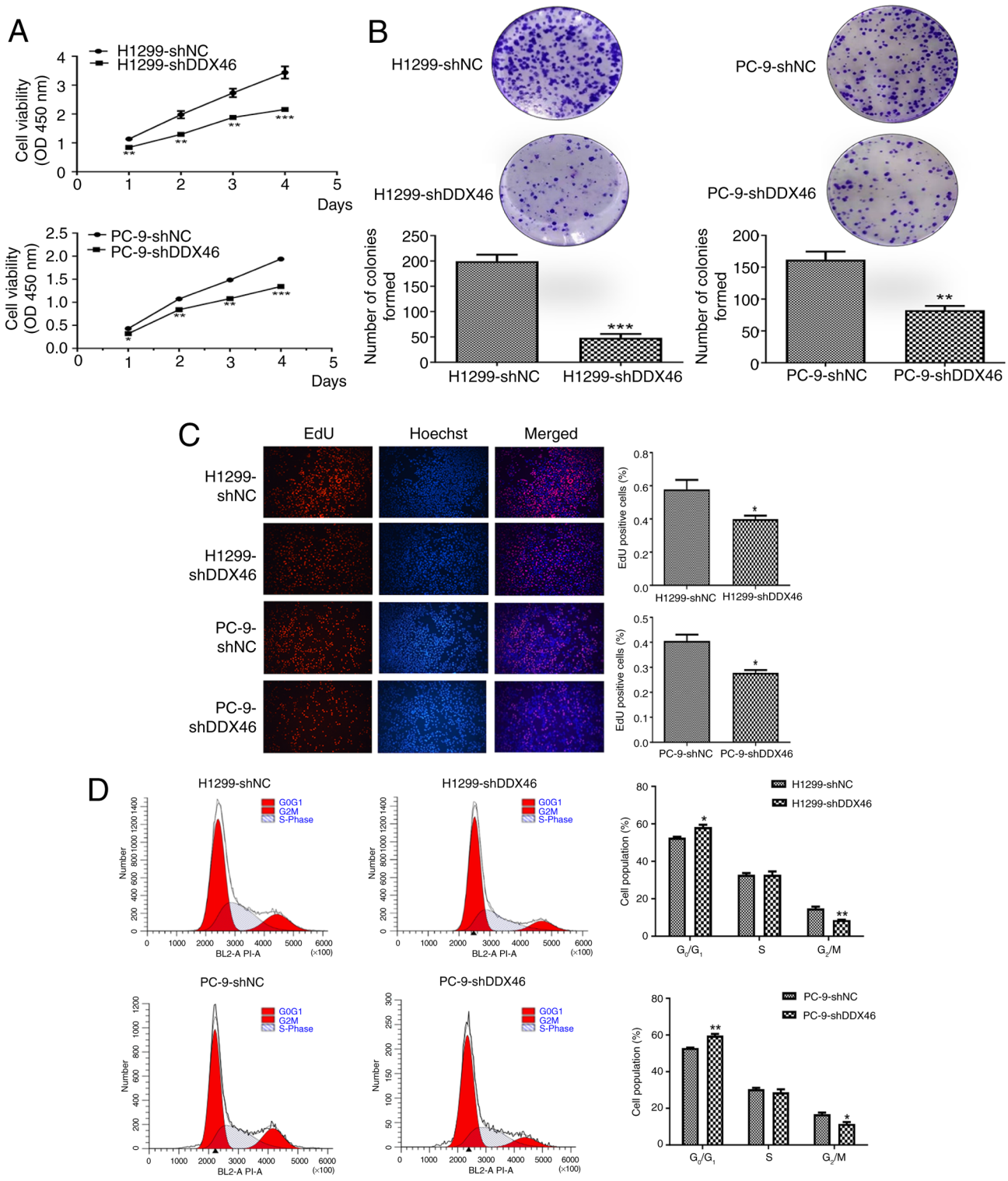

Figure 4. Knockdown of DDX46 inhibits the proliferation and cell cycle of lung adenocarcinoma cells. The proliferation of cells after knockdown of DDX4 was evaluated using Cell Counting Kit-8 assays in (A) H1299 andPC-9 cells, colony formation assays in (B) H1299 andPC-9 cells, and (C) EdU assays in both cell lines (magnification, x100). Cell cycle analysis was performed using (D) H1299 and PC-9 cells after knockdown of DDX46. *P<0.05; **P<0.01; ***P<0.001. DDX46, DEAD-box 4; EdU, 5-ethynyl-2'-deoxyuridine; sh, short hairpin; NC, negative control; OD, optical density.

GSEA analysis. In addition, KEGG pathway annotation was performed using the data (Table SII). The screening criteria were as follows: P<0.05 and FDR <0.05. The KEGG analysis results indicate that DDX46 is closely associated with the Wnt signaling pathway in LUAD (Fig. 6A). Subsequently, a list was compiled of the top 10 genes enriched in the Wnt signaling pathway by DDX46 (Fig. 6B). The analysis of the correlation between DDX46 and the top 10 genes in LUAD indicated that the gene with the strongest correlation was APC, with a correlation coefficient of 0.794 and a P-value of 6.28×10^{-113} (Fig. 6C). Furthermore, through western Blot analysis, it was further demonstrated that the expression of APC protein

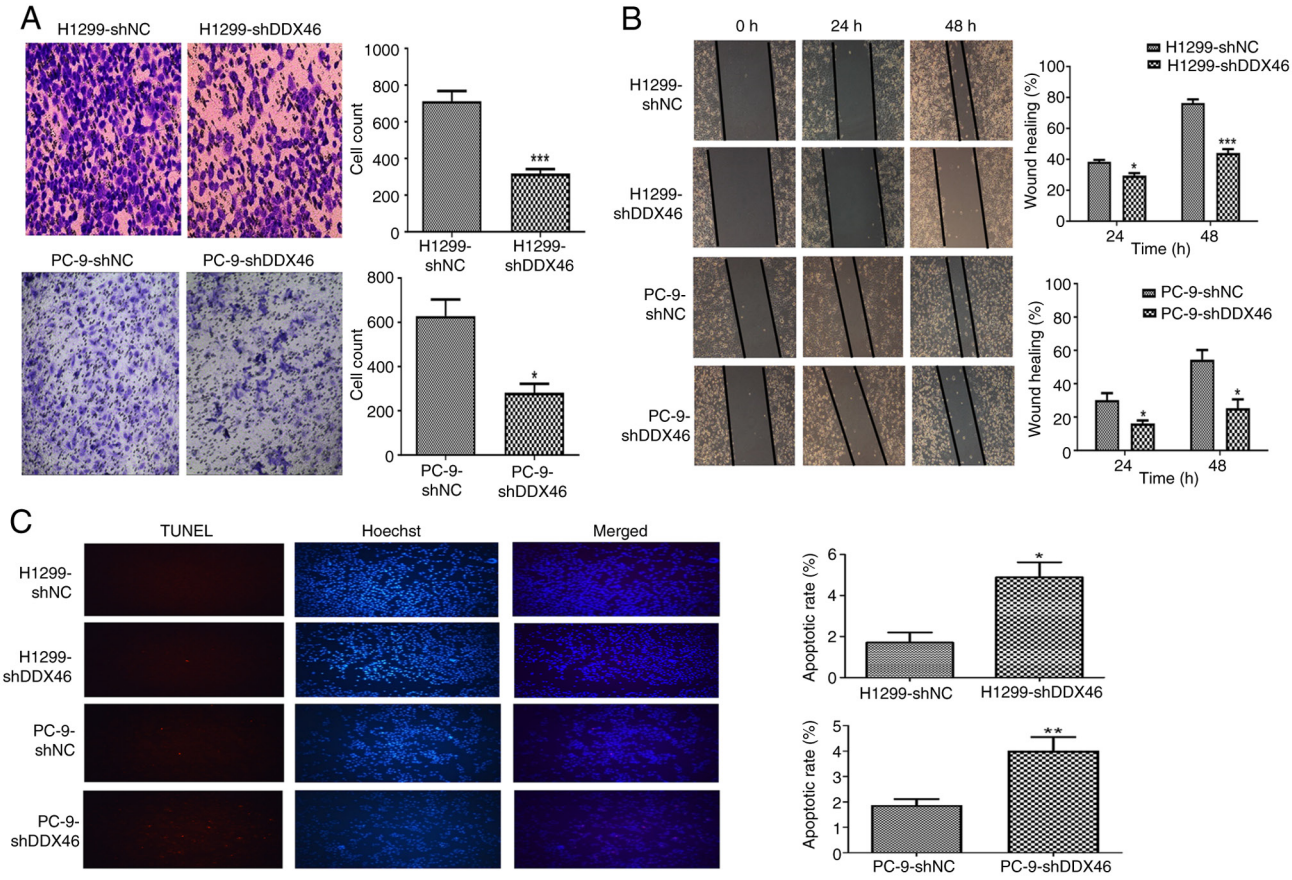

Figure 5. Inhibitory effect of silencing DDX46 on cell migration and apoptosis. Transwell migration assay performed in (A) H1299 and PC-9 cells, and the statistical analysis (magnification, x200). (B) Wound healing assays performed in H1299 and PC-9 cells, and the statistical analysis (magnification, x100). (C) Cell apoptosis assessed using TUNEL staining after DDX46 knockdown in H1299 and PC-9 cells (magnification, x100). *P<0.05; **P<0.01; ***P<0.001. DDX46, DEAD-box 4; sh, short hairpin; NC, negative control.

significantly increased whilst the expression of β-catenin protein significantly decreased in H1299 and PC-9 cells with DDX46 knockdown, in comparison with control cells (Fig. 6D and E). These results suggest that DDX46 is closely associated with the Wnt signaling pathway and may regulate the malignant progression LUAD through this pathway.

Association of DDX46 expression with immune infiltration. Analysis of the correlation between DDX46 and 8 major immune cells in LUAD revealed that DDX46 expression is significantly negatively correlated with CD8 T cells ($P=9.3x10^{-3}$; r=-0.12), regulatory T cells ($P=8.5x10^{-3}$; r=-0.12), follicular T cells ($P=2.7x10^{-3}$; r=-0.13) and natural killer (NK) cells ($P=2.6x10^{-3}$; r=-0.12), whilst it is significantly positively correlated with monocytes (P=0.02; r=0.11) (Fig. 7A). However, no correlation between the expression of DDX46 and B cells, CD4 T cells or macrophages was identified (Fig. S1). Furthermore, the GSE117570 dataset was used to determine the dominant cell types associated with DDX46 gene expression. The results demonstrated that the DDX46 gene is highly expressed in T cells, NK cells and monocyte subsets within the non-small cell LC microenvironment (Fig. 7B-D). Further correlation analysis between DDX46 expression and several immune checkpoints revealed that DDX46 is negatively correlated with cytotoxic T-lymphocyte associated protein 4 (CTLA4), Hepatitis A virus cellular receptor 2 (HAVCR2) and T cell immunoreceptor with Ig and ITIM domains (TIGIT) (Fig. 7E). Additionally, the relationship between DDX46 and several chemokines was analyzed. DDX46 was correlated with the expression of several chemokines, including CCL3, CCL5, CCL13, CCL15, CCL17, CCL19, CCL21, CCL23, CCL26, CX3CL1, CXCL1, CXCL8, CXCL16, CXCL17 and XCL2 (Fig. 7F). The correlation data between DDX46 and immune checkpoints and chemokines is presented in Tables SIII and SIV.

Analysis of DDX46 drug susceptibility. The association between DDX46 gene expression and the IC_{50} of commonly administered drugs in LUAD was assessed to ascertain whether the DDX46 gene is suitable for the personalized treatment of patients with LUAD. These commonly used drugs for LUAD treatment include AKT inhibitors, paclitaxel, crizotinib, erlotinib, gemcitabine, lapatinib, rapamycin and sorafenib. The findings revealed that patients with LUAD with low DDX46 expression demonstrated significantly increased sensitivity to some drugs (crizotinib, gemcitabine, lapatinib, paclitaxel and rapamycin), in comparison with those with high DDX46 expression. However, high expression of DDX46 may be associated with increased sensitivity to treatment with AKT inhibitors, erlotinib and sorafenib, potentially due to its impact on key cellular survival and proliferation pathways (Fig. 8).

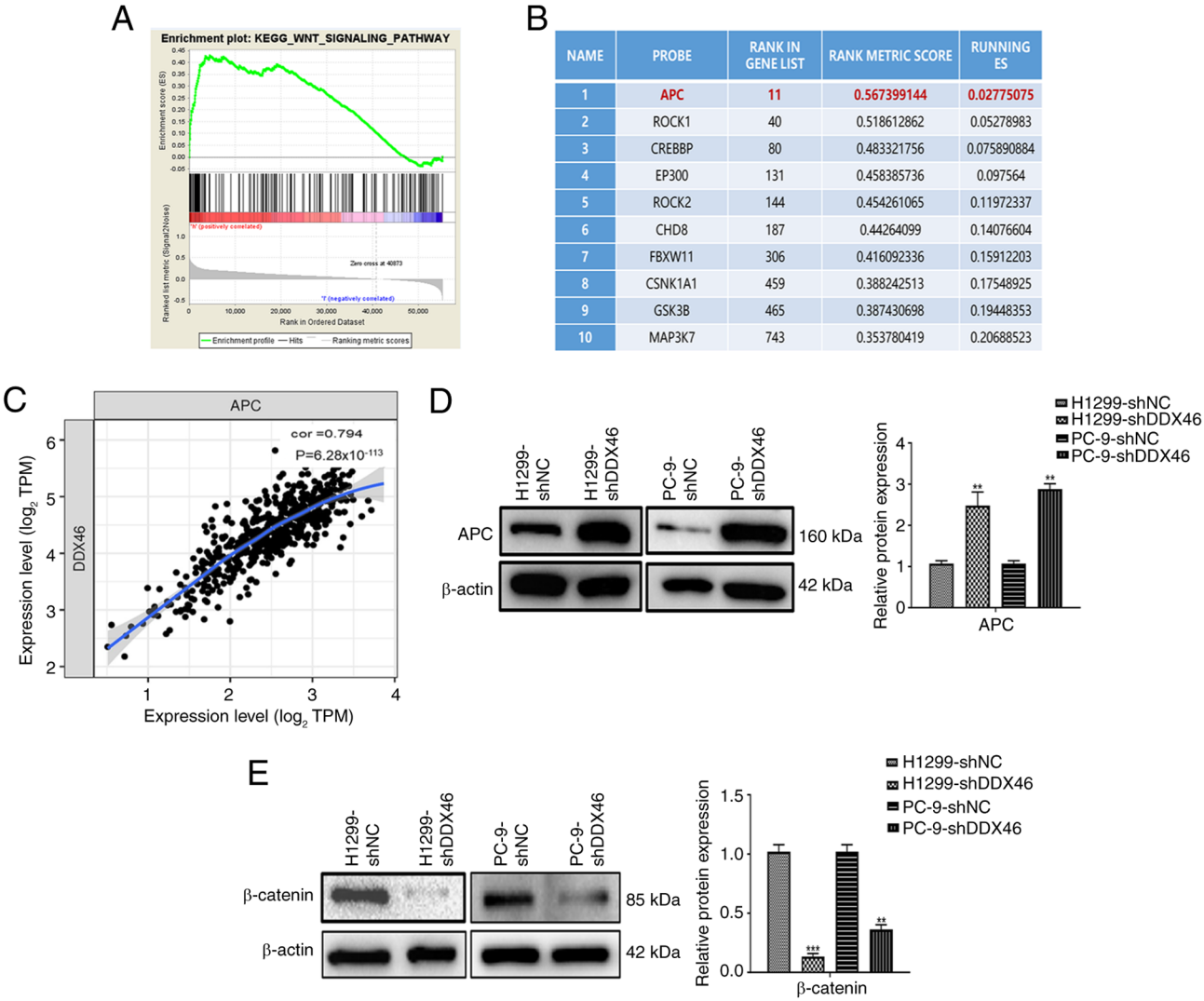

NAME	PROBE	RANK IN GENE LIST	RANK METRIC SCORE	RUNNING ES
1	APC	11	0.567399144	0.02775075
2	ROCK1	40	0.518612862	0.05278983
3	CREBBP	80	0.483321756	0.075890884
4	EP300	131	0.458385736	0.097564
5	ROCK2	144	0.454261065	0.11972337
6	CHD8	187	0.44264099	0.14076604
7	FBXW11	306	0.416092336	0.15912203
8	CSNK1A1	459	0.388242513	0.17548925
9	GSK3B	465	0.387430698	0.19448353
10	MAP3K7	743	0.353780419	0.20688523

Figure 6. DDX46 regulates the Wnt signaling pathway in LUAD cells. (A) DDX46 is closely associated with the Wnt signaling pathway in LUAD. (B) Top 10 genes enriched in the Wnt signaling pathway by DDX46. (C) Correlation analysis between DDX46 and APC in LUAD. In (D) H1299 and (E) PC-9 cells, western blot analysis revealed that APC protein expression increased after sh-DDX46 treatment, whilst β-catenin protein expression decreased, in comparison with sh-NC cells. **P<0.01; ***P<0.001. DDX46, DEAD-box 4; LUAD, lung adenocarcinoma; APC, adenomatous polyposis coli; sh, short hairpin; NC, negative control; KEGG, Kyoto Encyclopedia of Genes and Genomes; TPM, transcripts per million; cor, correlation coefficient; ES, enrichment score.

Discussion

The oncogenic role of DDX46 has been reported in several malignancies, including gastric cancer, colorectal cancer, esophageal squamous cell carcinoma and breast cancer (13,24,25). However, the specific biological function of DDX46 in LUAD progression and its relationship with immune infiltration and drug sensitivity remain poorly understood. The results of the present study demonstrated a significant upregulation of DDX46 in LUAD, which was associated with a poor prognosis. In LUAD cells, aberrant expression of DDX46 affected cell proliferation, invasion and migration. Bioinformatics analysis and experimental validation suggested that DDX46 may regulate the Wnt signaling pathway. Additionally, further bioinformatics analysis revealed that DDX46 is strongly linked to immune cell infiltration, immune checkpoints, chemokines and drug sensitivity.

Research has shown that the overexpression of DDX46 in human breast cancer is related to elevated histological grade and lymph node metastasis (25). In a parallel study on esophageal squamous cell carcinoma, a notable elevation in DDX46 expression was observed in both cancer cells and tissues (13). Additionally, colorectal cancer tissues have been reported to exhibit heightened focal nuclear DDX46 staining compared with adjacent normal tissues (24). Admoni-Elisha *et al* (26) reported an association correlation elevated DDX46 expression in patients with chronic lymphocytic leukemia and reduced OS. In the present research, the high expression of DDX46 in both LUAD tissues and cell lines was initially demonstrated, revealing its association with a poor prognosis. The findings suggest that DDX46 could serve as a valuable biomarker for stratifying patients with LUAD based on risk. By identifying patients with high DDX46 expression, clinicians could improve the prediction of those at higher risk of disease progression and poor outcomes. Functionally, abnormal expression of DDX46 contributes to enhanced proliferation, migration, invasion and suppressed apoptosis of esophageal squamous cell carcinoma, colorectal cancer cells

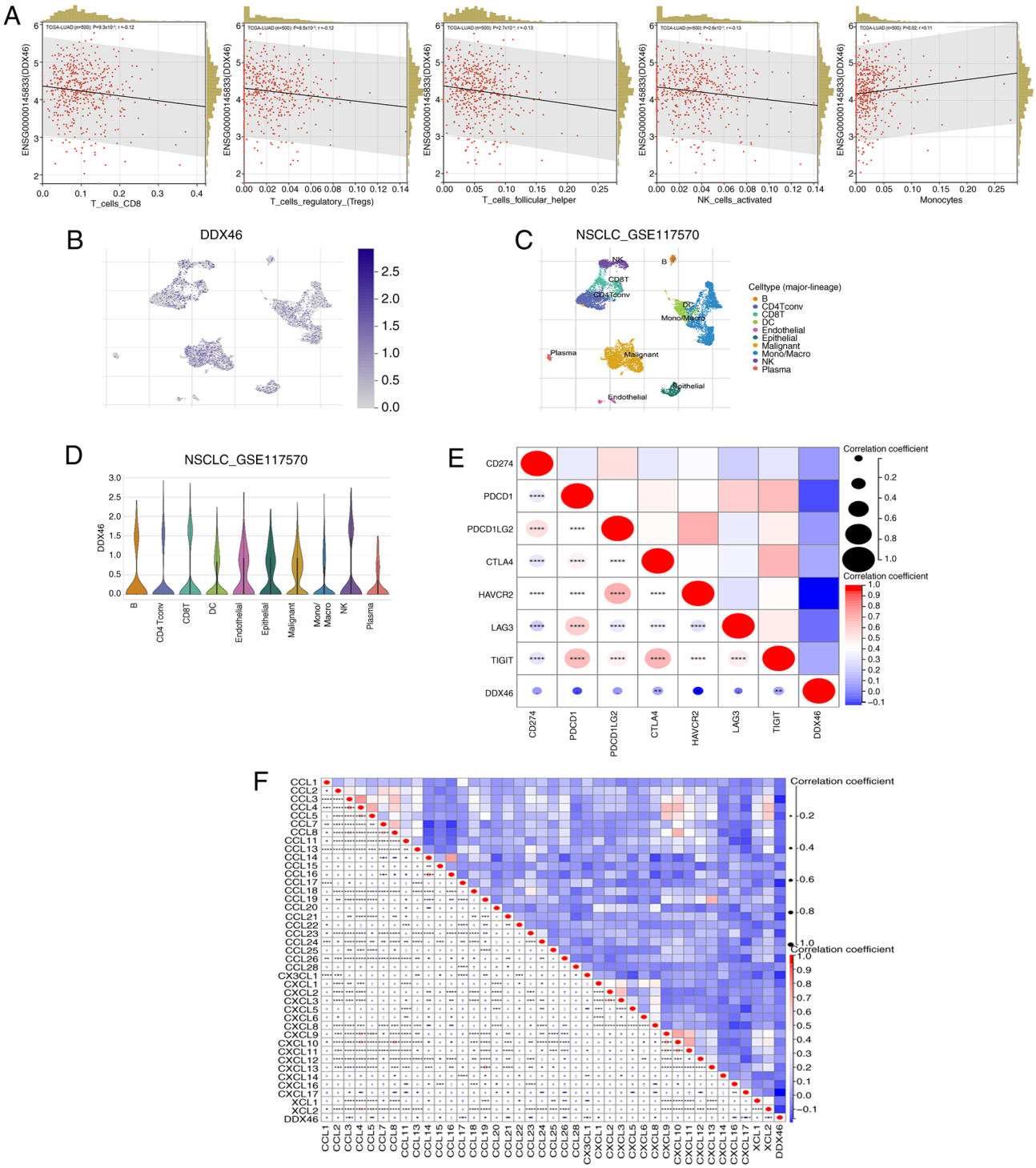

Figure 7. Immune infiltration analysis. (A) Correlation analysis between DDX46 expression and immune infiltrating cells in lung adenocarcinoma revealed that DDX46 expression is negatively correlated with CD8+ T cells, regulatory T cells, follicular T cells and NK cells, whilst it is positively correlated with monocytes. (B) Single-cell analysis demonstrated the expression of DDX46 in samples from the GSE117570 dataset. (C) UMAP plot of all cell clusters in the GSE117570 dataset. (D) Violin plots demonstrating the expression of DDX46 in each cell type in the GSE117570 dataset. Heat map analysis of the correlation between DDX46 expression and (E) immune checkpoints and (F) chemokines. ·P-value is not significant; *P<0.05; **P<0.01; ***P<0.001; ****P<0.0001. DDX46, DEAD-box 4; NK, natural killer; NSCLC, non-small cell lung cancer; DC, dendric cell.

and cutaneous squamous cell carcinoma *in vitro* and *in vivo* experiments (27). Additionally, in A549 cells, the interaction between structural maintenance of chromosomes 4 and the DDX46 gene was reported to impede cell M-phase progression, thereby inhibiting cell proliferation and invasion (28). The findings of the study align with the documented role of DDX46 in enhancing tumor cell proliferation, invasion and migration.

Prior research has reported that DDX46 influences the proliferation and migration of glioblastoma, gastric cancer and preeclampsia through the MAPK-p38, Akt/glycogen synthase kinase-3β/β-catenin and PI3K/Akt/mTOR signaling

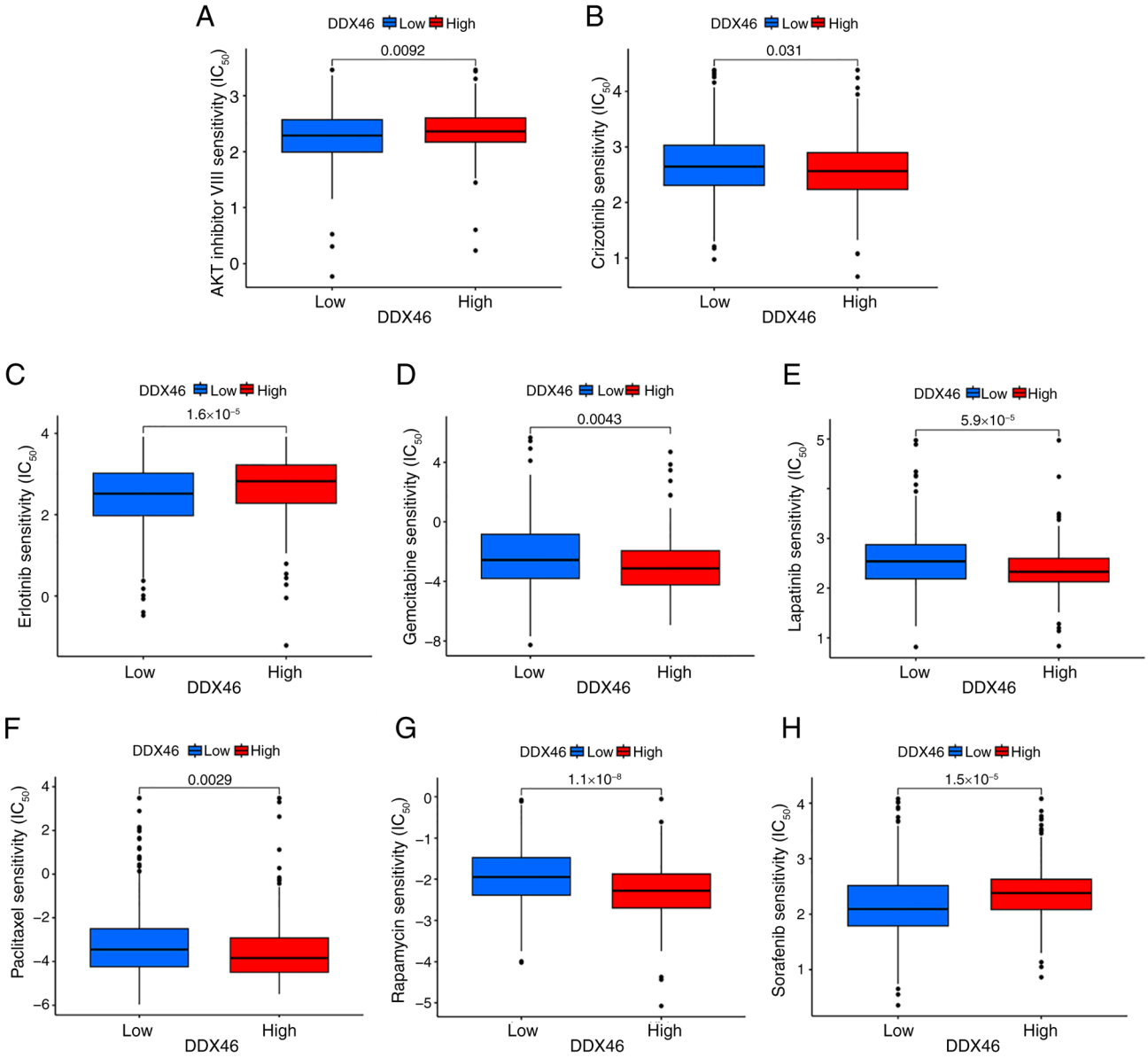

Figure 8. Drug sensitivity analysis of DDX46. Association of DDX46 with eight drugs: (A) AKT inhibitors, (B) crizotinib, (C) erlotinib, (D) gemcitabine, (E) lapatinib, (F) paclitaxel, (G) rapamycin and (H) sorafenib. DDX46, DEAD-box 46.

pathways (15,29,30). In the mechanism, KEGG pathway enrichment analysis revealed that DDX46 is strongly associated with the Wnt signaling pathway in LUAD. Correlation analysis also revealed that DDX46 has a high correlation coefficient with APC, in LUAD, reaching 0.794 with a P-value of $6.28x10^{-113}$. APC serves a critical suppressive role in the Wnt signaling pathway, and the interaction between APC and β-catenin is crucial for cell signaling, proliferation and fate determination. In cancer development, mutations in APC lead to the abnormal activation of β-catenin, a process that serves a critical role in tumorigenesis (31-34). In the present study, western blot analysis further demonstrated that, in H1299 and PC-9 cells with DDX46 knockdown, the expression of APC protein increased whilst the expression of β-catenin protein decreased. These findings offer fresh perspectives into the downstream regulatory mechanisms of DDX46 in tumor progression.

The present study revealed a strong association between DDX46 and diverse immune cells, immune checkpoints and chemokines. Immune cells and chemokines within the tumor immune microenvironment are pivotal in the pathogenesis of diverse tumors (35), with the degree of immune cell infiltration markedly impacting the prognosis of patients with solid tumors (36,37). Research has also reported that chemokines are involved in the circulation, homing, retention and activation of immune active cells (38,39). Notably, the findings of the present study indicate an inverse relationship between DDX46 expression and T cells, NK cells and immune checkpoints, CTLA4, HAVCR2 and TIGIT, suggesting a potential role for DDX46 in immune evasion. This mechanism could contribute to the progression of LUAD.

In the analysis of drug sensitivity associated with DDX46, it was revealed that DDX46 expression is associated with the sensitivity of cancer cells to several drugs, including AKT inhibitors, paclitaxel, crizotinib, erlotinib, gemcitabine, lapatinib, rapamycin and sorafenib. Numerous studies have

reported that the DDX helicase family proteins, in addition to their critical roles in RNA biology, can stimulate and bind to several protein kinases (40). This provides a theoretical basis for the influence of DDX46 expression on the sensitivity to multiple protein kinase inhibitors. AKT inhibitors are a class of targeted antitumor drugs that inhibit the AKT protein kinase (41). Previous studies have reported that knockdown of DDX46 can notably reduce the phosphorylation levels of AKT, thereby decreasing its kinase activity (14,15). Erlotinib, a tyrosine kinase inhibitor targeting the epidermal growth factor receptor (EGFR), inhibits tumor cell proliferation, survival and migration by blocking EGFR signaling pathways such as the Ras/Raf/MEK/ERK and PI3K/AKT/mTOR pathways (42). A study on preeclampsia also revealed that suppressing DDX46 inhibits trophoblast proliferation and migration through the PI3K/AKT/mTOR signaling pathway (30). Furthermore, a study on human colorectal cancer reported that the expression of DDX46 is associated with the apoptosis of tumor cells (24). One of the mechanisms of action of sorafenib is its ability to reduce the expression of anti-apoptotic proteins through multiple pathways, thereby promoting apoptosis (43). In summary, the impact of DDX46 expression on drug sensitivity or resistance in cancer cells is multifaceted, depending on the interplay between the mechanism of action of each drug and the cellular processes regulated by DDX46.

However, the present study has certain limitations. Although bioinformatics provides valuable insights and preliminary correlations, there is a lack of experimental validation to clarify the association between DDX46 and the Wnt signaling pathway. Similarly, the absence of *in vivo* experiments limits the ability to confirm the biological and mechanistic roles of DDX46 in LUAD. Future research should incorporate experiments targeting the Wnt signaling pathway and utilize animal models to validate the role of DDX46, establishing causal relationships with LUAD progression and immune regulation.

In conclusion, elevated DDX46 levels in patients LUAD may serve as a strong prognostic indicator and assist in diagnosis. Furthermore, high DDX46 expression promotes cell proliferation and survival in LUAD, highlighting its potential as a therapeutic target for diagnosis and treatment.

Acknowledgements

Not applicable.

Funding

The present research was funded by the National Natural Science Foundation of China (grant no. 82273422), the Nantong Basic Research Plan Project (grant no. MS2023067), the 2022 Nantong Basic Science Research and Social Livelihood Science and Technology Plan Project (grant no. MS22022111), the Research Project on Cutting-Edge Tumor Support Therapy (grant no. cphcf-2022-206), the Jiangsu Provincial Research Hospital (grant nos. YJXYY202204-YSC01 and YJXYY202204-YSB01) and the Key Project of Nantong's 14th Five Year Plan Science and Education Strengthening Health Project, Oncology Clinical Medical Center (grant no. NTYXZX18).

Availability of data and materials

The data generated in the present study may be requested from the corresponding author.

Authors' contributions

TB and MZ designed the study; TW, QZ and JZ performed the experiments; TW analyzed the data; TB and MZ wrote the paper and confirm the authenticity of all the raw data; YL and WS designed the work, drafted the manuscript and contributed to its revision. All authors read and approved the final version of the manuscript.

Ethics approval and consent to participate

The present study was performed in accordance with the Declaration of Helsinki and was approved by the Ethics Committee of the Affiliated Hospital of Nantong University (approval no. 2022-L078). The data were anonymous and the requirement for informed consent was waived.

Patient consent for publication

Not applicable.

Competing interests

The authors declare that they have no competing interests.

References

1. Collisson EA, Campbell JD, Brooks AN, Berger AH, Lee W, Chmielecki J, Beer DG, Cope L, Creighton CJ, Danilova L, *et al*: Comprehensive molecular profiling of lung adenocarcinoma: The cancer genome atlas research network. Nature 511: 543-550, 2014.
2. Chen P, Liu Y, Wen Y and Zhou C: Non-small cell lung cancer in China. Cancer Commun (Lond) 42: 937-970, 2022.
3. Zulfiqar B, Farooq A, Kanwal S and Asghar K: Immunotherapy and targeted therapy for lung cancer: Current status and future perspectives. Front Pharmacol 13: 1035171, 2022.
4. Herbst RS, Morgensztern D and Boshoff C: The biology and management of non-small cell lung cancer. Nature 553: 446-454, 2018.
5. Denisenko TV, Budkevich IN and Zhivotovsky B: Cell death-based treatment of lung adenocarcinoma. Cell Death Dis 9: 117, 2018.
6. Hooper C and Hilliker A: Packing them up and dusting them off: RNA helicases and mRNA storage. Biochim Biophys Acta 1829: 824-834, 2013.
7. Linder P and Jankowsky E: From unwinding to clamping-the DEAD box RNA helicase family. Nat Rev Mol Cell Biol 12: 505-516, 2011.
8. Owttrim GW: RNA helicases: Diverse roles in prokaryotic response to abiotic stress. RNA Biol 10: 96-110, 2013.
9. Robert F and Pelletier J: Perturbations of RNA helicases in cancer. Wiley Interdiscip Rev RNA 4: 333-349, 2013.
10. Steimer L and Klostermeier D: RNA helicases in infection and disease. RNA Biol 9: 751-771, 2012.
11. Abdelhaleem M, Maltais L and Wain H: The human DDX and DHX gene families of putative RNA helicases. Genomics 81: 618-622, 2003.
12. Will CL, Urlaub H, Achsel T, Gentzel M, Wilm M and Lührmann R: Characterization of novel SF3b and 17S U2 snRNP proteins, including a human Prp5p homologue and an SF3b DEAD-box protein. EMBO J 21: 4978-4988, 2002.
13. Li B, Li YM, He WT, Chen H, Zhu HW, Liu T, Zhang JH, Song TN and Zhou YL: Knockdown of DDX46 inhibits proliferation and induces apoptosis in esophageal squamous cell carcinoma cells. Oncol Rep 36: 223-230, 2016.

14. Jiang F, Zhang D, Li G and Wang X: Knockdown of DDX46 inhibits the invasion and tumorigenesis in osteosarcoma cells. Oncol Res 25: 417-25, 2017.
15. Chen L, Xu M, Zhong W, Hu Y and Wang G: Knockdown of DDX46 suppresses the proliferation and invasion of gastric cancer through inactivating Akt/GSK-3β/β-catenin pathway. Exp Cell Res 399: 112448, 2021.
16. Wang Z, Jensen MA and Zenklusen JC: A practical guide to the cancer genome atlas (TCGA). Methods Mol Biol 1418: 111-141, 2016.
17. Zheng M, Liu J, Bian T, Liu L, Sun H, Zhou H, Zhao C, Yang Z, Shi J and Liu Y: Correlation between prognostic indicator AHNAK2 and immune infiltrates in lung adenocarcinoma. Int Immunopharmacol 90: 107134, 2021.
18. Livak KJ and Schmittgen TD: Analysis of relative gene expression data using real-time quantitative PCR and the 2(-Delta Delta C(T)) method. Methods 25: 402-408, 2001.
19. Sun D, Wang J, Han Y, Dong X, Ge J, Zheng R, Shi X, Wang B, Li Z, Ren P, *et al*: TISCH: A comprehensive web resource enabling interactive single-cell transcriptome visualization of tumor microenvironment. Nucleic Acids Res 49 (D1): D1420-D1430, 2021.
20. Lei Y, Zhou B, Meng X, Liang M, Song W, Liang Y, Gao Y and Wang M: A risk score model based on lipid metabolism-related genes could predict response to immunotherapy and prognosis of lung adenocarcinoma: A multi-dataset study and cytological validation. Discov Oncol 14: 188, 2023.
21. Ru B, Wong CN, Tong Y, Zhong JY, Zhong SSW, Wu WC, Chu KC, Wong CY, Lau CY, Chen I, *et al*: TISIDB: An integrated repository portal for tumor-immune system interactions. Bioinformatics 35: 4200-4202, 2019.
22. Komuro H, Shinohara S, Fukushima Y, Demachi-Okamura A, Muraoka D, Masago K, Matsui T, Sugita Y, Takahashi Y, Nishida R, *et al*: Single-cell sequencing on $CD8^+$ TILs revealed the nature of exhausted T cells recognizing neoantigen and cancer/testis antigen in non-small cell lung cancer. J Immunother Cancer 11: e007180, 2023.
23. Yang W, Soares J, Greninger P, Edelman EJ, Lightfoot H, Forbes S, Bindal N, Beare D, Smith JA, Thompson IR, *et al*: Genomics of drug sensitivity in cancer (GDSC): A resource for therapeutic biomarker discovery in cancer cells. Nucleic Acids Res 41 (Database Issue): D955-D961, 2013.
24. Li M, Ma Y, Huang P, Du A, Yang X, Zhang S, Xing C, Liu F and Cao J: Lentiviral DDX46 knockdown inhibits growth and induces apoptosis in human colorectal cancer cells. Gene 560: 237-244, 2015.
25. Ma Z, Song J, Hua Y, Wang Y, Cao W, Wang H and Hou L: The role of DDX46 in breast cancer proliferation and invasiveness: A potential therapeutic target. Cell Biol Int 47: 283-291, 2023.
26. Admoni-Elisha L, Nakdimon I, Shteinfer A, Prezma T, Arif T, Arbel N, Melkov A, Zelichov O, Levi I and Shoshan-Barmatz V: Novel biomarker proteins in chronic lymphocytic leukemia: Impact on diagnosis, prognosis and treatment. PLoS One 11: e0148500, 2016.
27. Lin Q, Jin HJ, Zhang D and Gao L: DDX46 silencing inhibits cell proliferation by activating apoptosis and autophagy in cutaneous squamous cell carcinoma. Mol Med Rep 22: 4236-4242, 2020.
28. Zhang C, Kuang M, Li M, Feng L, Zhang K and Cheng S: SMC4, which is essentially involved in lung development, is associated with lung adenocarcinoma progression. Sci Rep 6: 34508, 2016.
29. Ma J, Gao Z and Liu X: DDX46 accelerates the proliferation of glioblastoma by activating the MAPK-p38 signaling. J BUON 26: 2084-2089, 2021.
30. You X, Cui H, Yu N and Li Q: Knockdown of DDX46 inhibits trophoblast cell proliferation and migration through the PI3K/Akt/mTOR signaling pathway in preeclampsia. Open Life Sci 15: 400-408, 2020.
31. Disoma C, Zhou Y, Li S, Peng J and Xia Z: Wnt/β-catenin signaling in colorectal cancer: Is therapeutic targeting even possible? Biochimie 195: 39-53, 2022.
32. Wan C, Mahara S, Sun C, Doan A, Chua HK, Xu D, Bian J, Li Y, Zhu D, Sooraj D, *et al*: Genome-scale CRISPR-Cas9 screen of Wnt/β-catenin signaling identifies therapeutic targets for colorectal cancer. Sci Adv 7: eabf2567, 2021.
33. Zhan T, Rindtorff N and Boutros M: Wnt signaling in cancer. Oncogene 36: 1461-1473, 2017.
34. Hankey W, Frankel WL and Groden J: Functions of the APC tumor suppressor protein dependent and independent of canonical WNT signaling: Implications for therapeutic targeting. Cancer Metastasis Rev 37: 159-172, 2018.
35. Bai R, Yin P, Xing Z, Wu S, Zhang W, Ma X, Gan X, Liang Y, Zang Q, Lei H, *et al*: Investigation of GPR143 as a promising novel marker for the progression of skin cutaneous melanoma through bioinformatic analyses and cell experiments. Apoptosis 29: 372-392, 2024.
36. Ino Y, Yamazaki-Itoh R, Shimada K, Iwasaki M, Kosuge T, Kanai Y and Hiraoka N: Immune cell infiltration as an indicator of the immune microenvironment of pancreatic cancer. Br J Cancer 108: 914-923, 2013.
37. Schneider K, Marbaix E, Bouzin C, Hamoir M, Mahy P, Bol V and Gregoire V: Immune cell infiltration in head and neck squamous cell carcinoma and patient outcome: A retrospective study. Acta Oncol 57: 1165-1172, 2018.
38. Franciszkiewicz K, Boissonnas A, Boutet M, Combadiere C and Mami-Chouaib F: Role of chemokines and chemokine receptors in shaping the effector phase of the antitumor immune response. Cancer Res 72: 6325-6332, 2012.
39. Koizumi K, Hojo S, Akashi T, Yasumoto K and Saiki I: Chemokine receptors in cancer metastasis and cancer cell-derived chemokines in host immune response. Cancer Sci 98: 1652-1658, 2007.
40. Hirth A, Fatti E, Netz E, Acebron SP, Papageorgiou D, Švorinić A, Cruciat CM, Karaulanov E, Gopanenko A, Zhu T, *et al*: DEAD box RNA helicases are pervasive protein kinase interactors and activators. Genome Res 34: 952-966, 2024.
41. Shariati M and Meric-Bernstam F: Targeting AKT for cancer therapy. Expert Opin Investig Drugs 28: 977-988, 2019.
42. Wu SG and Shih JY: Management of acquired resistance to EGFR TKI-targeted therapy in advanced non-small cell lung cancer. Mol Cancer 17: 38, 2018.
43. Wu CH, Lin KH, Fu BS, Hsu FT, Tsai JJ, Weng MC and Pan PJ: Sorafenib induces apoptosis and inhibits NF-κB-mediated anti-apoptotic and metastatic potential in osteosarcoma cells. Anticancer Res 41: 1251-1259, 2021.